Polymer Journal (2015) 47, 819–825

www.nature.com/pj

ORIGINAL ARTICLE

Silk 3D matrices incorporating human neural progenitor cells for neural tissue engineering applications

Bano Subia[1], Raj R Rao[2] and Subhas C Kundu[1]

The fabrication of cytocompatible and porous three-dimensional (3D) biomaterial scaffolds is one of the main goals of neural tissue engineering. Silk fibroin 3D scaffolds from mulberry and non-mulberry silks were designed to bridge the tissue gap and provide structural support to maintain the native function of the normal tissues. The microstructure of the fabricated fibroin scaffolds was evaluated which revealed relatively homogeneous pore structure and interconnectivity. The pore sizes and porosity of the scaffolds ranged from 105 to 112 μm and from 90 to 95%, respectively. The 3D scaffolds were examined by culturing human neural progenitor cells, which demonstrated good cell viability and proliferation over 14 days. The cell culture, hematoxylin–eosin and immunocytochemical results demonstrate that the matrices provided cytocompatibility, good cell morphology and maximum matrix deposition, with the 3D silk-based scaffolds designed from both sources producing comparable results. Although not significantly different, non-mulberry silk matrices appeared to promote slightly increased cell proliferation and matrix deposition. These results indicate that the silk matrices may serve as potential biomaterials for neural regeneration and tissue engineering applications.
Polymer Journal (2015) **47,** 819–825; doi:10.1038/pj.2015.69; published online 2 September 2015

INTRODUCTION

Damage to the central nervous system in mammals occurs owing to disease or trauma that leads to a limited ability to restore normal anatomy and function.[1] Neural tissue engineering seeks to develop effective treatment strategies to regenerate lost nerve function using approaches designed to restore the original tissue structure and function.[2] For the successful growth/repair of diseased or damaged tissue, designed scaffolds, cells and stimulatory growth factors are needed. Tissue engineering often uses conventional biomaterials to engineer tissues that mimic the natural extracellular matrix (ECM).[3] The natural ECM is a complex mixture of structural and functional proteins and can be used as an inspiration for the development of active tissue-engineered scaffolds. This approach has been proposed as a potential alternative for the treatment of central nervous system disorders that are incapable of neural regeneration owing to a lack of matrix and proper structural support.[4,5] It has been demonstrated that the interaction of transplanted or migrated stem cells with the ECM has a key role in neural tissue regeneration and healing. For this reason, it is necessary to bridge the tissue gap and provide structurally supported substrates.[6,7] In addition, it is necessary to support neurogenesis and regenerate lost brain tissue in cases of large abrasions and a lack of donor tissue replacement.[8] Scaffold-based implants may be more resistant to transplantation and more useful for achieving successful neural tissue regeneration and implantation.[9,10] Tissue engineering requires porous scaffolds as a temporary support for neo-tissue generation that should be degraded when the support is no longer needed.[11,12] Scaffolds with three-dimensional (3D) fibrous architectures, high surface areas and interconnected porosity are needed for neural cell adhesion, infiltration, proliferation, differentiation and neurite elongation.[1,13]

The 3D scaffolds prepared from the fibrous silk protein fibroin, isolated from mulberry *Bombyx mori* and non-mulberry Indian tropical tasar silkworm *Antheraea mylitta,* have been utilized for a number of biomedical and biotechnological applications, as they show excellent biological compatibility, mechanical strength and biodegradability.[14,15] Fibroin is considered to be a suitable material for skeletal, bone, cartilage, neural and other hard tissue engineering applications. Silk matrices show good oxygen and water-vapor permeabilities and exhibit minimal inflammatory reactions *in vivo*.[16] Fibroin shows controlled degradability, mechanical robustness and stimulates neural cell growth and proliferation.[17,18] Fibroin is an excellent candidate for a variety of *in vitro* and *in vivo* applications in neural tissue engineering owing to its biocompatibility and easy processability.[19] In addition to matrices (that is, temporary ECM), soluble growth factors also influence neurite cell growth and differentiation.[20] The matrix protein poly-L-ornithine, laminin

[1]Department of Biotechnology, Indian Institute of Technology Kharagpur, Kharagpur, India and [2]Department of Chemical and Life Science Engineering, Virginia Commonwealth University, Richmond, VA, USA
Correspondence: Professor SC Kundu, Department of Biotechnology, Indian Institute of Technology Kharagpur, Kharagpur, West Bengal 721302, India.
E-mail: kundu@hijli.iitkgp.ernet.in
or Professor RR Rao, Department of Chemical and Life Science Engineering, Virginia Commonwealth University, Richmond, Virginia 23284-3028, USA.
E-mail: rrrao@vcu.edu or
Received 3 March 2015; revised 24 June 2015; accepted 10 July 2015; published online 2 September 2015

and stimulatory growth factors such as basic fibroblast growth factors and leukemia inhibitory factors have been used to increase neurogenesis, neurite extension and stimulate neural cell differentiation *in vitro*.[21,22]

Human neural progenitor (hNP) cells are emerging as attractive cell sources for neural tissue engineering and cell-based therapies for diseases affecting the central and peripheral nervous systems. We previously demonstrated the ability to generate hNP cells that can be continuously propagated *in vitro*, maintain a stable karyotype, multipotency and are capable of differentiation into neurons, oligodendrocytes and astrocytes.[23–28] Conventional two-dimensional culture systems are generally used for the growth and expansion of hNP cells but have limitations owing to improper cellular interactions.[14] The 3D scaffolds provide a unique microenvironment that mimics the *in vivo* environment of the cells and provides cell–cell and cell–matrix interactions for proper structural support and migration.[29]

Mulberry silk is well characterized and is more widely used for tissue engineering applications than any other silk. Here, mulberry silk was used for a comparative study with non-mulberry silk. However, non-mulberry silks have not been utilized as widely as mulberry silks in different aspects. A recent report on non-mulberry silk from the species *Antheraea mylitta* (Am) showed additional advantages owing to its higher mechanical strength and the existence of integral RGD sequences. This property helped to improve cell adhesion.[30] Because of their superior cell adhesion and proliferation properties, this material and other non-mulberry silks are attracting attention for use in different applications as biomaterials.[31–34] Thus, in this study, 3D silk protein fibroin scaffolds were designed from both mulberry (*Bombyx mori*) and non-mulberry tropical tasar (*Antheraea mylitta*) silk sources and used to investigate the growth and proliferation of hNP cells. Multiple experimental outcomes indicated that the cultured hNP cells proliferated within the 3D scaffolds and could potentially be used to promote neural regeneration as part of neural tissue engineering strategies.

MATERIALS AND METHODS

Materials

Mulberry silk cocoons of *Bombyx mori* (Bm) from a local silk farm and non-mulberry Am larvae were obtained from our IIT Kharagpur local farms, District of West Midnapore, State of West Bengal, India. Na_2CO_3 (Merck, Kolkata, India), LiBr (Merck), SDS (Merck), dialysis tubing (molecular weight cut-off 12 kDa), neural basal medium (Life Technologies, Grand Island, NY, USA), B27 serum supplement, poly-L-ornithine, laminin, basic fibroblast growth factors and leukemia inhibitory factors (Millipore, Billerica, MA, USA), Nestin and DAPI (4',6-diamidino-2-phenylindole) were acquired from commercial vendors. All the materials were obtained from Sigma Chemicals, St Louis, MO, USA (unless otherwise noted).

Preparation of silk fibroin solution from Bm

Silk protein fibroin protein was isolated from the cocoons of Bm following a standard extraction protocol with slight modification. Briefly, the cocoons were cut into small pieces, boiled with 0.02 M Na_2CO_3 for 60 min and washed with deionized water several times to remove sericin from the silk fibers. The degummed fibers were then dried completely. The degummed fibers were dissolved in 9.3 M LiBr at 60 °C for 4 h. The regenerated silk fibroin solution was then dialyzed in cellulose tubing (12 kDa molecular weight cut-off) against deionized water for 48 h to remove the remaining lithium bromide. The fibroin solution was then centrifuged at 9000 r.p.m. for 10 min to remove undissolved materials, and the final solution was collected. The concentration of fibroin was determined by gravimetric and colorimetric (Bradford) analysis.

Isolation of fibroin from *Antheraea mylitta* (Am)

The fully grown 5th instar larvae, just prior to spinning, were dissected to extract fibroin according to previously published methods.[34] The procedure followed to obtain the fibroin solution from BM cocoons did not allow us to obtain sufficient protein; thus, fibroin was isolated from the glands of the silkworms just prior to being spun into cocoons. Briefly, the silk glands were isolated and washed in deionized water to remove traces of sericin. The glandular tubes were then squeezed with fine forceps to extrude out the fibroin. The isolated fibroin was dissolved using a mild anionic surfactant, SDS, and the surfactant was removed by dialysis against water using a dialysis membrane. The fibroin solution was collected, and the concentration was determined by gravimetric and colorimetric (Bradford) analysis.

Fibroin scaffold preparation and processing

The scaffolds were prepared by a freeze-drying method, with a pre-freezing temperature of −20 °C. When newly lyophilized fibroin scaffolds were rehydrated in neutral aqueous medium, they exhibited rapid swelling and ultimately dissolved. The scaffolds were rehydrated in an ethanol series such as 100% (15 min) followed by 70% (30 min). This protocol helps the fibroin to form β-sheets, which prevent the fibroin from dissolving in water or cell culture medium.[33] After this step, the scaffolds were washed with sterile PBS (pH 7.4) three times in a laminar flow hood to remove the alcohol, followed by washing with cell culture medium, after which they were used for cell culture.

Characterization of the fibroin scaffolds

Scanning electron microscopy. Freeze-dried silk scaffolds were sectioned and sputter coated with gold, and their morphology was observed with a JEOL-JSM 5800 scanning electron microscopy. The pore sizes of both untreated and ethanol-treated fibroin scaffolds were determined using Image J software (NIH, USA), and a minimum of 30 pores were examined for each type of scaffold generated.

Pore size and porosity of the fibroin scaffolds. The porosity of the fibroin scaffolds from Bm and Am was measured by the liquid displacement method. The scaffolds were immersed in a known volume (V_1) of hexane in a graduated cylinder for 5 min. The total volume of hexane and the hexane-impregnated scaffold was recorded as V_2. The hexane-impregnated scaffolds were then removed from the cylinder, and the residual hexane volume was recorded as V_3. For all types of scaffolds, experiments were carried out in triplicate. The porosity of the scaffold ε was obtained by

$$\text{Porosity}(\varepsilon) = (V_1 - V_3/V_2 - V_3) \times 100,$$

where V_1 = known volume of hexane, V_2 = total volume of scaffolds and hexane-impregnated scaffolds and V_3 = residual hexane volume after removal of scaffolds.

Brunauer, Emmett and Teller surface area analysis. The Brunauer, Emmett and Teller procedure, which is based on the adsorption of inert gas, was used to measure the total surface area of the scaffolds. Gas molecules of known sizes were condensed into the unknown sample surface. To completely cover the surface and open pores of each particle with condensed gas, a surface area analyzer was used to characterize the surface, including irregularities and pore interiors, down to an atomic level. The 'out-gassed' samples of silk, placed under high vacuum in a sample tube, were immersed in a coolant bath of liquid nitrogen at −196 °C. At this stage, the sample was ready to attract gas molecules into its surface. The amount of gas adsorbed and the resultant sample pressure was recorded. The data were analyzed to obtain the surface area.

Fourier transform infrared spectroscopy analysis

Confirmation of the transitions in alcohol-treated and untreated fibroin films were obtained using a Perkin Elmer Fourier transform infrared spectrometer over the spectral region of 500–4000 cm^{-1} at a resolution of 4 cm^{-1}. All the samples were measured by the absorbance method, and spectra were recorded at room temperature and analyzed with Microcal Origin Version 6.0.

Maintenance of cell culture

The hNP cells (Aruna Biomedical, Athens, GA, USA) were obtained and routinely characterized, as per published protocols.[23] The cells were routinely cultured on poly-L-ornithine (20 μg ml^{-1}) and laminin (5 μg ml^{-1}) coated 35 mm Petri dishes. Briefly, the cells were cultured in neural basal medium (GIBCO) supplemented with B27 serum (5%), the growth factors like leukemia inhibitory factor (50 μl) and basic fibroblast growth factors (40 μl), and 100 U ml^{-1} of penicillin/streptomycin and glutamine. The cells were incubated at 37 °C and 5% CO_2 under sterile conditions. To study the growth and proliferation, the hNP cells were seeded at a density of 5×10^4 cells/scaffolds in a 24-well tissue culture plate in complete neural basal medium for 24 h. The culture medium was replaced every day with fresh neural basal medium.

Immunocytochemical analysis

Immunocytochemical analysis was performed to determine the expression of surface antigens on hNPs cultured in the scaffolds. The hNP samples were rinsed in phosphate-buffered saline (PBS), fixed in ice-cold 4% PFA for 10 min and then washed with sterile PBS. After permeabilization with 0.025% Triton X-100, the cells were incubated with 2.5% normal goat serum in PBS for 30 min at 37 °C to prevent nonspecific binding. After washing with PBS three times (5 min each), the cells were incubated with primary antibody (Nestin, cell surface markers, 1:100 dilution) for 3 h in the dark at 4 °C. After staining, PBS (pH 7.4) washing was performed three times, after which the cells were incubated with a fluorescently labeled secondary anti-mouse antibody at room temperature for 2 h. The cell nuclei were counterstained with DAPI, and the samples were analyzed by confocal microscopy.

Cell seeding

The 3D porous aqueous-derived pure fibroin scaffolds (2 mm thick and 6 mm in diameter) were carefully seeded in 24-well plates with 5×10^4 neural progenitor cells suspended in serum-containing medium. The constructs were kept in a 37 °C incubator for 3 h to allow the cells to diffuse into and attach to the scaffolds before adding fresh medium to the wells. One milliliter of neural basal medium was added to empty wells in the seeding plates to maintain humid conditions in the culture plate. After 3 h, 200 μl culture medium was added into each well for the growth of cells. The cultures were replenished with and thereafter maintained in complete neural basal medium, with the medium being replaced every day. The cultures were harvested at day 14 for analysis.

Cell proliferation assay. The cell proliferation was assessed using the Alamar blue assay following the manufacturers' instructions (Life Technologies, Invitrogen, Carlsbad, CA, USA). Alamar blue is a non-toxic, aqueous fluorescent dye that does not affect cell viability and proliferation. Briefly, the cell-seeded scaffolds were incubated in medium supplemented with 10% (v/v) Alamar blue fluorescent dye (Biosource, Camarillo, CA, USA) for 4 h. Two hundred microliters of medium from each experimental condition was read at 570/600 nm in a Multiskan spectrum plate reader (Thermo Electron Corporation, Waltham, MA, USA). Non-seeded scaffolds supplemented with 10% Alamar blue dye were used as a negative control. The percentage of Alamar blue (AB) reduction (%AB reduction) was calculated as follows:

$$\%\text{ABreduction} = \left[\frac{(\varepsilon_{ox}\lambda_2)(A\lambda_1) - (\varepsilon_{ox}\lambda_1)(A\lambda_2)}{(\varepsilon_{red}\lambda_1)(A'\lambda_2) - (\varepsilon_{red}\lambda_2)(A'\lambda_1)}\right] \times 100,$$

where $\varepsilon\lambda_1$ and $\varepsilon\lambda_2$ represent the molar extinction coefficient of Alamar blue at 570 and 600 nm, in the oxidized (ε_{ox}) and reduced (ε_{red}) forms, respectively, $A\lambda_1$ and $A\lambda_2$ denote the absorbance of the test wells at 570 and 600 nm, respectively, while $A'\lambda_1$ and $A'\lambda_2$ denote the absorbance of the negative control wells, at the same wavelengths.

Confocal microscopy. Attachment of hNP cells on fibroin scaffolds was assessed using confocal microscopy. The matrices were seeded with 6×10^4 hNP cells/scaffold and cultured for 7 days in neural basal medium. After 7 days, the matrices were harvested and the cells were fixed in 4% paraformaldehyde and washed with PBS (pH 7.4) three times. The samples were then permeabilized using 0.1% Triton X-100 for 5 min and washed with PBS. The samples were incubated with rhodamine–phalloidin for 30 min at room temperature, followed by washing with PBS and staining with 5 μg m^{-1} Hoechst 33342 for 30 min. Fluorescence images of stained constructs were obtained using a confocal laser scanning microscope equipped with argon (488 nm) and helium–neon (534 nm) lasers. Two-dimensional multichannel image processing was carried out using FV 1000 Advance software v. 1.6 (Olympus, New York, NY, USA).

Tissue processing

The cell-seeded scaffold constructs were fixed with 4% paraformaldehyde in PBS, embedded in paraffin and sectioned using a microtome. Multiple sections were observed under microscopy to evaluate the expression of hNP cells by histology and immunohistochemistry. A section thickness of 5 μm was used, and slides were stained with hematoxylin–eosin to visualize the histology. For immunohistochemistry, the scaffolds were fixed with 4% paraformaldehyde, cryosectioned and blocked with 2.5% normal horse serum for 30 min, and the constructs were incubated with mouse monoclonal antibody against nestin (cell surface marker). Subsequently, cells within the scaffolds were incubated with biotinylated goat anti-mouse antibody, reacted with ABC reagent containing avidin–horseradish peroxidase (vectastain elite universal ABC kit, Vectors Lab, Burlingame, CA, USA). The samples were then stained with the peroxidase substrate 3,3′-diaminobenzidine (DAB) and H_2O_2 to develop a brown color. The sections were counterstained with methyl green and then observed on an inverted microscope (Nikon eclipse TS100, Haverhill, MA, USA).

Statistical analysis

Significant differences were determined using a one-way analysis of variance. Data are presented as the mean ± s.d. *P*-values <0.05 were considered as statistically significant.

RESULTS AND DISCUSSION

Scaffolds porosity and surface area analysis

The pore architecture of scaffolds is known to have a critical role in tissue engineering, as it provides the vital framework for the seeded cells to organize into a functioning tissue. Small pore sizes lead to reduced porosity and insufficient swelling, thereby inhibiting nutrient transfer, whereas larger pore sizes hinder cell attachment and affect overall cell viability and can also lead to excess swelling and structural deformation. Controlling the pore size is critical for optimal swelling, which is essential for maximizing nutrient allocation without compromising the overall structural integrity.[35] The morphologies of fibroin scaffolds prepared from mulberry Bm and Indian tropical tasar silkworm non-mulberry Am were analyzed from scanning electron microscopy pictographs. The Am and Bm scaffolds with and without ethanol treatment were highly porous and the pores were interconnected, as shown in Figure 1. The pore sizes of the Bm and Am scaffolds were in the range of 110 ± 4 and 120 ± 8 μm for untreated and 105 ± 6 and 112 ± 5 μm for treated scaffolds (Figure 1). The liquid displacement method was used to measure the porosity of the scaffolds by using hexane as the displacement liquid. The porosities of the Am and Bm scaffolds were 82 ± 12 and 85 ± 8 %, respectively. The surface areas of the scaffolds obtained from $scCO_2$ drying were 480 and 520 m^2 g^{-1} for Am and Bm scaffolds, respectively. The scaffolds had similar porosity, indicating that the source of the scaffold did not affect the porosity or surface area under similar processing conditions. Scanning electron microscopy images showed that the pore size, surface area and porosity of the scaffolds facilitated the growth and proliferation of hNP cells. The 3D fibroin scaffolds provided proper structural support to the hNP cells. The pore size and porosity of the scaffold help the cells to receive biochemical cues from the culture medium. In addition, the scaffolds may be efficient for delivering mechanical signals to the adherent cells.[36] Hexane was chosen to measure the porosity of both the fibroin scaffolds because it permeates the scaffolds without causing much

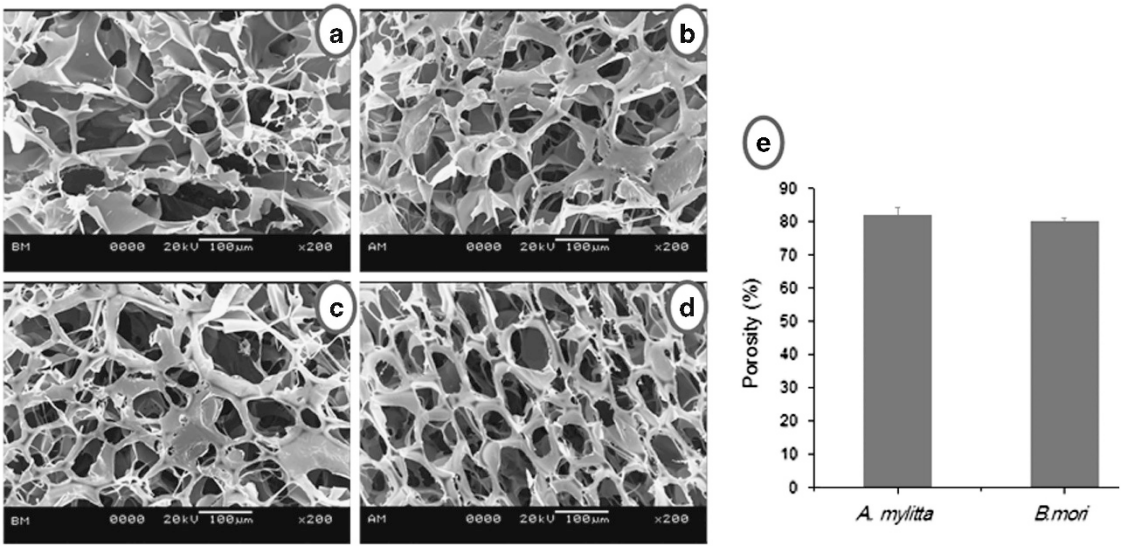

Figure 1 Scanning electron microscopy images of untreated (**a**) *A. mylitta* and (**b**) *B. mori* and ethanol-treated (**c**) *A. mylitta* and (**d**) *B. mori* scaffolds. (**e**) Porosity percentages of the scaffolds. Each point represents the mean ± s.d. ($n=3$). A full color version of this figure is available at *Polymer Journal* online.

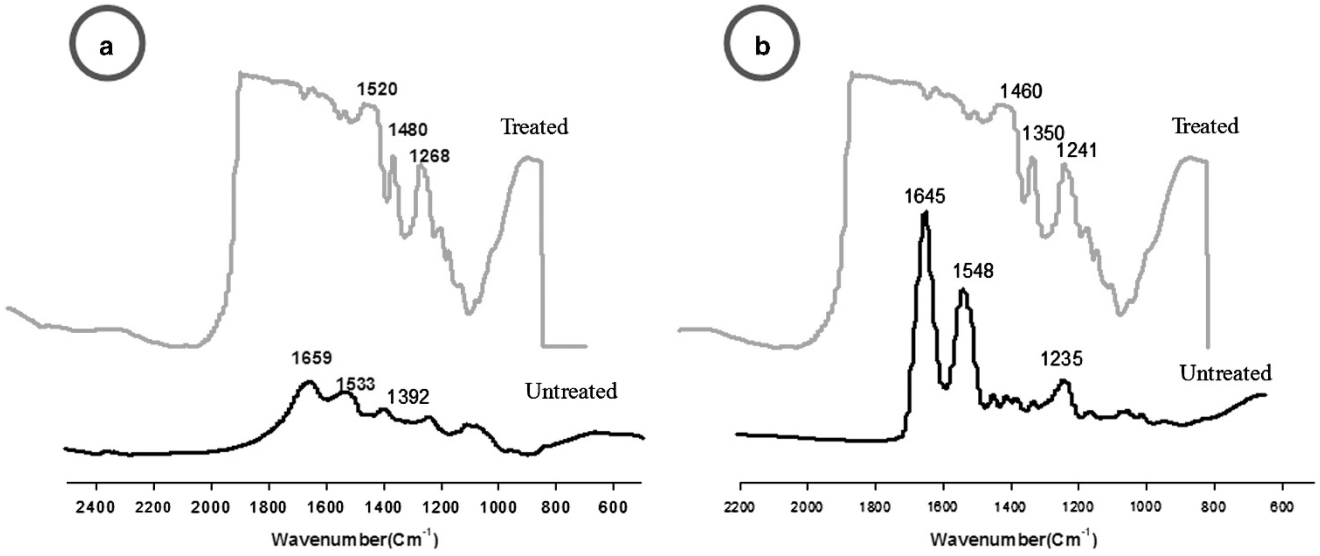

Figure 2 FTIR (Fourier transform infrared) spectroscopy analysis of the silk fibroin proteins of untreated and ethanol-treated (**a**) *A. mylitta* and (**b**) *B. mori* silk. Black lines represent the untreated group and the red line represents ethanol-treated scaffolds. A full color version of this figure is available at *Polymer Journal* online.

shrinkage or swelling compared to other liquids, such as ethanol.[37] The porosity, pore size of the scaffolds and the culture of hNP cells were not affected by the processing conditions used in this study. The pore size, porosity and surface area of the scaffolds were functionally competent for delivering a platform for neural tissue engineering.

Fourier transform infrared spectroscopy analysis of the scaffolds

Fourier transform infrared spectroscopy was used to analyze the presence of secondary structure in the protein after processing. Silk protein fibroin molecules have their characteristic bands in the spectral regions of amide I from 1600 to 1700 cm^{-1} (C=O stretching) and amide II from 1500 to 1600 cm^{-1} (N–H bending). Our results indicate that the fibroin of *A. mylitta* and *B. mori* possessed the characteristic amide I (1659 and 1645 cm^{-1}, respectively) and amide II bands (1533 and 1548 cm^{-1}) in these absorption regions, as shown in Figure 2. The fibroins of *A. mylitta* and *B. mori* when treated with ethanol showed the characteristic amide I (1520 and 1460 cm^{-1}) and amide II bands (1480 and 1350 cm^{-1}, respectively). The secondary structural confirmation results indicate that alpha helical structure of untreated fibroin was changed into a crystalline structure after treatment with ethanol, as shown in Figure 2, indicating that the silk fibroin protein is structurally stable after ethanol treatment and can also be used for long-term cell culture.

Immunocytochemical analysis and confocal microscopy

Immunocytochemical analysis indicated that the hNP cells maintained positive expression of Nestin under routine culture conditions, as

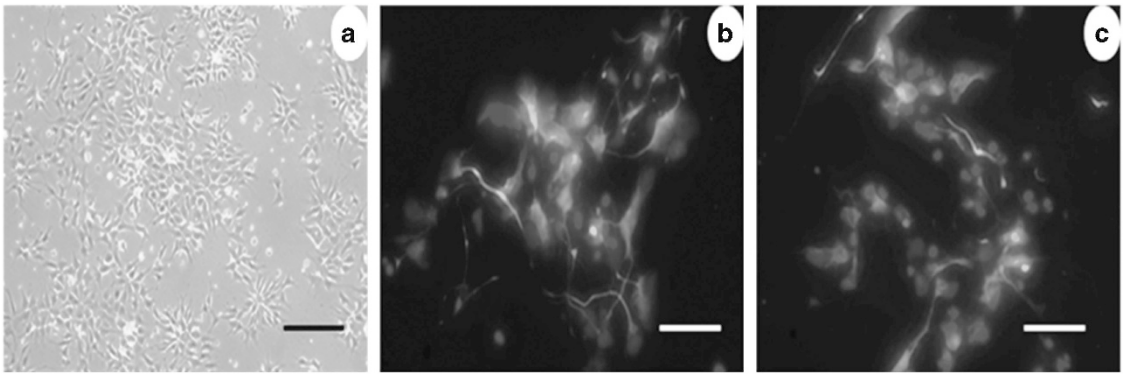

Figure 3 Fluorescent micrographs showing immunostaining of the neural progenitor cells. (**a**) Unstained neural progenitor cells. (**b**, **c**) Neural progenitor cells stained for the cell surface marker nestin (green color) and with DAPI (4',6-diamidino-2-phenylindole) for nuclear staining (blue color) (**b**, **c**). Scale bar represents 100 μm. A full color version of this figure is available at *Polymer Journal* online.

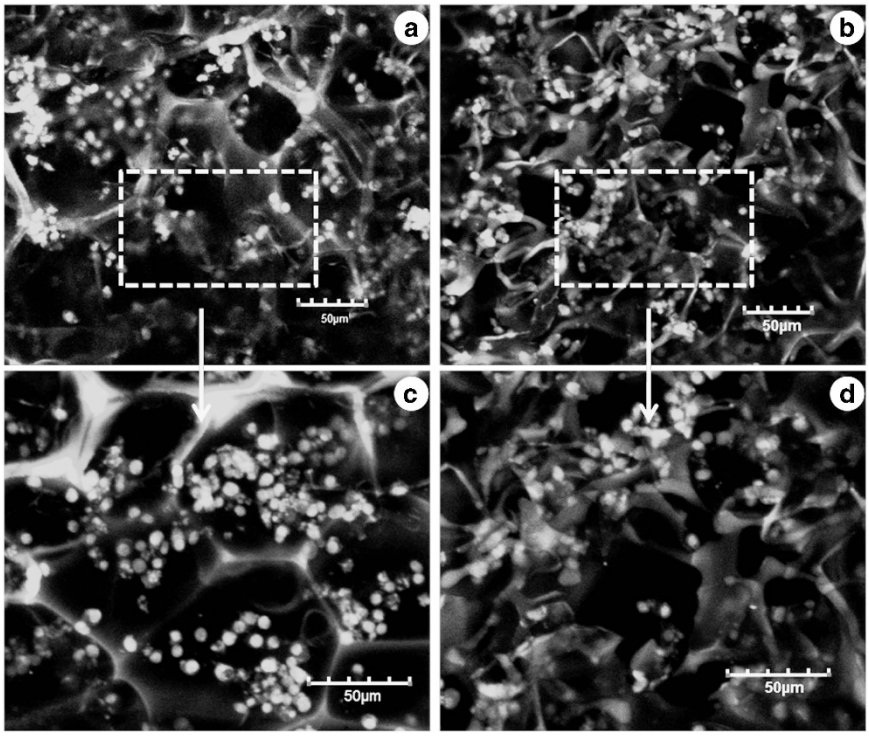

Figure 4 Confocal laser micrographs showing cell growth and proliferation on 3D fibroin scaffolds of non-mulberry *A. mylitta* (**a**, **c**) and mulberry *B. mori* (**b**, **d**) sources. The cells were stained with rhodamine–phalloidin for actin filaments (green) and DAPI (4',6-diamidino-2-phenylindole) for nuclear staining (blue). Scale bars represent 50 μm. A full color version of this figure is available at *Polymer Journal* online.

shown in Figure 3, indicating that the hNP cells proliferate and maintain the characteristics of progenitor cells.

Cell attachment on the silk fibroin-based 3D scaffolds was evaluated using confocal laser microscopy. After 7 days of culture in neural basal medium, hNPs on both scaffolds showed good cell attachment and distribution. The hNP cells are routinely passaged in neural basal medium supplemented with B27, basic fibroblast growth factor and leukemia inhibitory factor. Staining of the nuclei with DAPI dye indicated proper growth, as shown in Figure 4. These confocal microscopy observations demonstrate that the hNP cells were able to grow and proliferate in the 3D scaffold-based culture system and maintained their geometry after a week of culture. However, the hNP cells on the non-mulberry scaffolds showed greater cell attachment and proliferation compared with the mulberry scaffolds, probably due to the presence of RGD sequences, which mediate cell attachment, in the non-mulberry silk fibroin.[38] These results confirm that hNP cells robustly interact with the surrounding ECM.

Cell proliferation assay

Proliferation of hNP cells in the 3D fibroin of *A. mylitta* and *B. mori* was observed up to 14 days of cell culture, as shown in Figure 5. The proliferation rate of the hNPs on the 3D scaffolds of *A. mylitta* was higher compared with the *B. mori* scaffolds. In the *A. mylitta* scaffolds, the hNPs first demonstrated rapid proliferation and showed a higher peak from day 1 to 5, after which the hNPs continued to proliferate on both the silk scaffolds at a constant rate (Figure 5). There was not

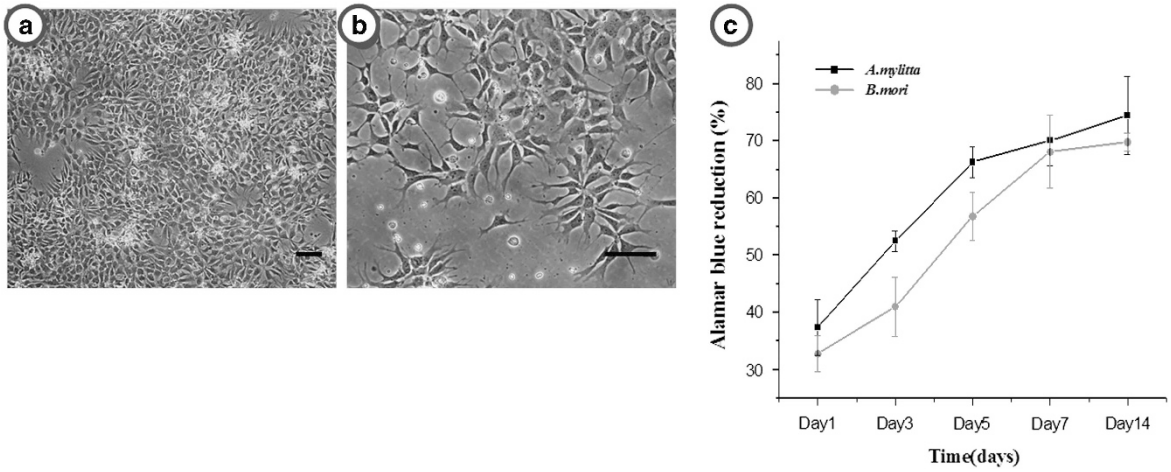

Figure 5 Cell growth and morphology of the human neural progenitor cells (**a**, **b**; scale bar represents 100 μm). Proliferation of human neural progenitor cells on *A. mylitta* and *B. mori* 3D scaffolds after 14 days (**c**). A full color version of this figure is available at *Polymer Journal* online.

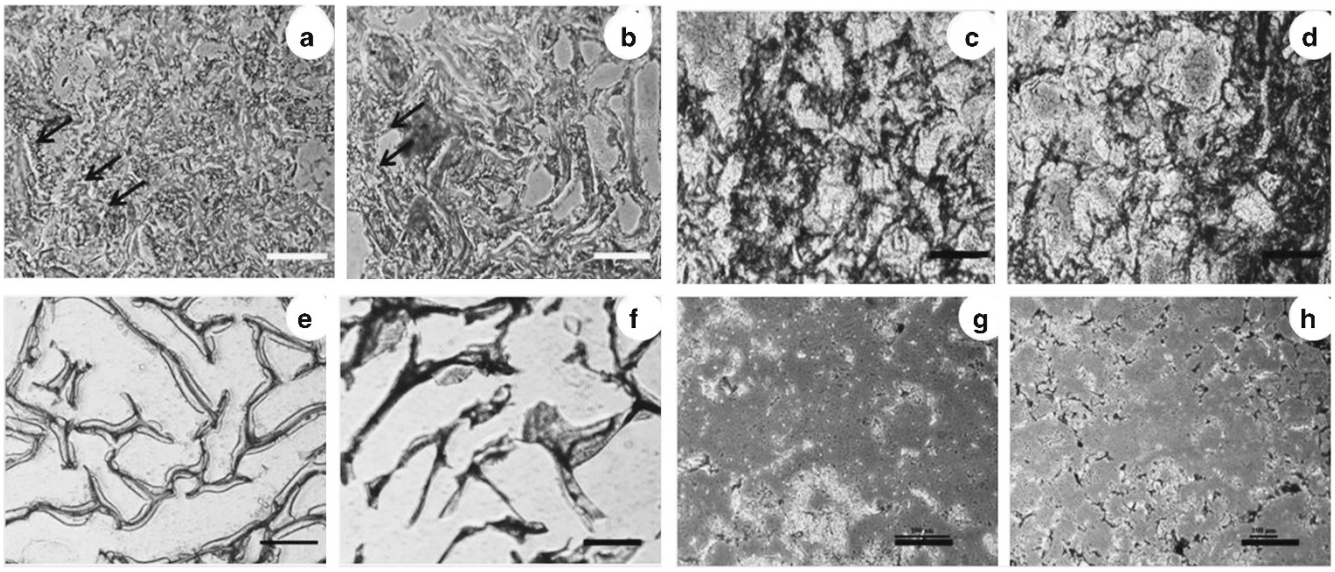

Figure 6 H&E (hematoxylin–eosin) staining of human neural progenitor cells seeded on *A. mylitta* (**a**), *B. mori* scaffolds (**b**) and non-seeded scaffolds from *A. mylitta* and *B. mori* (**e**, **f**). Immunohistochemical staining of neural progenitor cells on 3D scaffolds from *A. mylitta* (**c**) and *B. mori* (**d**), and non-seeded scaffolds from *A. mylitta* (**g**) and *B. mori* (**h**). Scale bar represents 100 μm. A full color version of this figure is available at *Polymer Journal* online.

much difference in the proliferation rate of hNPs on the silk fibroin scaffolds of *B. mori* and *A. mylitta*. However, minor differences in the cell proliferation rate may be owing to the presence of the RGD sequences in *A. mylitta* fibroin. This difference might promote hNP cell adhesion and proliferation within the scaffolds.[39] These observations indicate that the silk fibroin biomaterial matrices can serve as supportive scaffolds, modulate the behavior of cells[1,40,41] and may also be used to temporarily fill injury sites and support cell growth.

Histology and immunohistochemistry

Histological analysis demonstrated the proliferation of hNP cells on the 3D matrices of *A. mylitta* and *B. mori*, as observed after hematoxylin and eosin staining. In Figure 6, after being cultured for 7 days, cell nuclei were clearly visible in both the sectioned scaffolds. Immunohistochemical staining revealed positive expression of Nestin based on the deep brown color of the DAB (3,3'-diaminobenzidine tetra hydrochloride) reagent. Non-seeded constructs showed less or no expression of nestin. Overall, these results indicate that the cells were well distributed in both silk fibroin 3D matrices. Nestin positive cells were also observed in both the matrices, as identified by immunohistochemistry (Figure 6). This newly generated ECM component supports the growth, proliferation and successful migration of hNP cells within the matrices.

CONCLUSIONS

The biocompatible and biodegradable 3D silk fibroin scaffolds from Indian tropical tasar silkworm non-mulberry *Antheraea mylitta* and mulberry *Bombyx mori* provided structural support for hNP cells. They also provided a neuro-anatomical and functional microenvironment for the culture of hNP cells. The silk matrices supported hNP cell survival, proliferation and also enhanced matrix deposition and the expression of nestin, a classic hNP marker. These findings

demonstrate that the silk fibroin-based matrices can potentially be used for neural regeneration and other biomedical applications. Further studies are needed to evaluate the potential application of the 3D scaffolds for promoting differentiation into specialized neuronal subtypes for neural tissue engineering applications.

CONFLICT OF INTEREST

The authors declare no conflict of interest.

ACKNOWLEDGEMENTS

This work was supported by the Department of Biotechnology and its Bioinformatics facility (SCK and for fellowship to BS) and the Qimonda Endowment Award from Virginia Commonwealth University, USA (RRR). We are grateful to colleagues in the Department of Chemical and Life Science Engineering, Virginia Commonwealth University USA, for their support during our (BS and SCK) short stay. RRR also acknowledges support from the VCU Global Education Office for a short visit to the Department of Biotechnology, Indian Institute of Technology Kharagpur, India.

1 Wang, Y., Yao, M., Zhou, J., Zheng, W., Zhou, C., Dong, D., Liu, Y., Teng, Z., Jiang, Y., Wei, G. & Cui, X. The promotion of neural progenitor cells proliferation by aligned and randomly oriented collagen nanofibers through b1 integrin/MAPK signaling pathway. *Biomaterials* **32**, 6737–6744 (2011).
2 Apple, A. A., Anastasio, M. A., Larson, J. C. & Brey, A. M. Imaging challenges in biomaterials and tissue engineering. *Biomaterials* **34**, 6615–6630 (2013).
3 Seidi, A., Ramalingam, M., Elloumi-Hannachi, I., Ostrovidov, S. & Khademhosseini, A. Gradient biomaterials for soft-to-hard interface tissue engineering. *Acta Biomater.* **7**, 1441–1451 (2011).
4 Modo, M., Stroemer, R. P., Tang, E., Patel, S. & Hodges, H. Effects of implantation site of stem cell grafts on behavioral recovery from stroke damage. *Stroke* **33**, 2270–2280 (2002).
5 Lo, E. H., Dalkara, T. & Moskowitz, M. A. Mechanisms, challenges and opportunities in stroke. *Nat. Rev. Neurosci.* **4**, 399–415 (2003).
6 Baiguera, S., Gaudio, C. D., Lucatelli, E., Kuevdac, E., Boieri, M., Mazzanti, B., Bianco, A. & Macchiarini, P. Electrospun gelatin scaffolds incorporating rat decellularized brain extracellular matrix for neural tissue engineering. *Biomaterials* **35**, 1205–1214 (2013).
7 Viapiano, M. S. & Matthews, R. T. From barriers to bridges: chondroitin sulfate proteoglycans in neuropathology. *Trends Mol. Med.* **12**, 488–496 (2006).
8 Park, K. I., Teng, Y. D. & Snyder, E. Y. The injured brain interacts reciprosically with neural stem cells supported by scaffolds to reconstitute lost tissue. *Nat. Biotechnol.* **20**, 1111–1117 (2002).
9 Li, Y. C., Tsai, L. K., Wang, J. H. & Young, T. H. A neural stem/precursor cell monolayer for neural tissue engineering. *Biomaterials* **35**, 1192–1204 (2014).
10 Ai, J., Kiasat-Dolatabadi, A., Ebrahimi- Barough, S., Ai, A. & Lotfibakhshaiesh, N. Polymeric scaffolds in neural tissue engineering: a review. *Arch. Neuro. Sci.* **1**, 1–20 (2013).
11 Liang, Y., Walczak, P. & Bulte, J. W. M. The survival of engrafted neural stem cells within hyaluronic acid hydrogels. *Biomaterials* **34**, 5521–5529 (2013).
12 Guo, B., Sun, Y., Finne-Wistrand, A., Mustafa, K. & Albertsson, A. C. Electroactive porous tubular scaffolds with degradability and non-cytotoxicity for neural tissue regeneration. *Acta Biomater.* **8**, 144–153 (2012).
13 Guo, B. L., Finne-Wistrand, A. & Albertsson, A. C. Enhanced electrical conductivity by macromolecular architecture: hyperbranched electroactive and degradable block copolymers based on poly(epsilon-caprolactone) and aniline pentamer. *Macromolecules* **43**, 4472–4480 (2010).
14 Zhang, H. & Kohn, D. H. Using polymeric materials to control stem cell behaviour for tissue regeneration. *Birth Def. Res. C* **96**, 63–68 (2012).
15 Subia, B., Chandra, S., Talukdar, S. & Kundu, S. C. Folate conjugated silk fibroin nanocarriers for targeted drug delivery. *Integr. Biol.* **6**, 203–214 (2014).
16 Yun, S. H., Byun, K., Bhin, J., Oh, J. H., Nhungle, T. H., Hwang, D. & Lee, B. Transcriptional regulatory network associated with self renewal and differentiation of neural stem cells. *J. Cell Physiol.* **225**, 337–347 (2010).
17 Tsukada, S., Nakashima, H. & Torimitsu, K. Conductive polymer combined silk fiber bundle for bioelectrical signal recording. *PLoS ONE* **7**, e33689 (2012).
18 Subia, B. & Kundu, S. C. Drug loading and release on tumor cells using silk fibroin-albumin nanoparticles as carriers. *Nanotechnology* **24**, 035103 (2013).
19 Chlapanidas, T., Faragò, S., Mingotto, F., Crovato, F., Tosca, M. C., Antonioli, B., Bucco, M., Lucconi, G., Scalise, A., Vigo, D., Faustini, M., Marazzi, M. & Torre, M. L. Regenerated silk fibroin scaffold and infrapatellar adipose stromal vascular fraction as feeder-layer: a new product for cartilage advanced therapy. *Tissue Eng. A* **17**, 1725–1733 (2011).
20 Lam, H. J., Patel, S., Wang, A., Chu, J. & Li, S. In vitro regulation of neural differentiation and axon growth by growth factors and bioactive nanofibers. *Tissue Eng. A* **16**, 2641–2648 (2010).
21 Nelson, A. D. & Svendsen, C. N. Low concentrations of extracellular FGF-2 are sufficient but not essential for neurogenesis from human neural progenitor cells. *Mol. Cell Neurosci.* **33**, 29–45 (2006).
22 Rydel, R. & Greene, L. Acidic and basic fibroblast growth factors promote stable neurite outgrowth and neuronal differentiation in cultures of PC12 cells. *J. Neurosci.* **7**, 3639–3649 (1987).
23 Dhara, S. K., Hasneen, K., Machacek, D. W., Boyd, N. L., Rao, R. R. & Stice, S. L. Human neural progenitor cells derived from embryonic stem cells in feeder-free cultures. *Differentiation* **76**, 454–464 (2008).
24 Iyer, S., Alsayegh, K., Abraham, S. & Rao, R. R. Stem cell based models and therapies for neurodegenerative diseases. *Crit. Rev. Biomed. Eng.* **37**, 321–353 (2009).
25 Iyer, S., Xiao, E., Alsayegh, K., Riggs, M. J., Eroshenko, N., Bennett, J. P. & Rao, R. R. Mitochondrial Gene replacement in human pluripotent stem cell derived neural progenitors. *Gene Ther.* **19**, 469–475 (2012).
26 Wilczynska, K. M., Singh, S. K., Adams, B., Bryan, L. E., Rao, R. R., Valerie, K., Wright, S., Griswold-Prenner, I. & Kordula, T. Nuclear Factor I isoforms regulate gene expression during the differentiation of human neural progenitors to astrocytes. *Stem Cells* **27**, 1173–1181 (2009).
27 Shin, S., Mitalipova, M., Noggle, S., Tibbitts, D., Venable, A., Rao, R. R. & Stice, S. L. Long term proliferation of human embryonic stem cell-derived neuroepithelial cells using defined adherent culture conditions. *Stem Cells* **24**, 125–138 (2006).
28 Dodla, M., Young, A., Johnson, A. V., Hasneen, K., Rao, R. R., Machacek, D. & Stice, S. L. Differing lectin binding profiles among human embryonic stem cells and derivatives aid in the isolation of neural progenitor cells. *PLoS ONE* **6**, e23266 (2011).
29 Geckil, H., Xu, F., Zhang, X., Moon, S. & Demirci, U. Engineering hydrogel as extracellular matrix mimics. *Nanomedicine* **5**, 469–484 (2010).
30 Patra, C., Talukdar, S., Novoyatleva, T., Velagala, S. R., Mühlfeld, C., Kundu, B., Kundu, S. C. & Engel, F. B. Silk protein fibroin from *Antheraea mylitta* for cardiac tissue engineering. *Biomaterials* **33**, 2673–2680 (2012).
31 Pal, S., Kundu, J., Talukdar, S., Thomas, T. & Kundu, S. C. An emerging functional natural silk biomaterial from the only domesticated nonmulberry silkworm *Samia ricini*. *Macromol. Biosci.* **13**, 1020–1035 (2013).
32 Liu, Y., Xiong, S., You, R. & Li, M. Gelation of *Antheraea pernyi* silk fibroin accelerated by shearing. *J. Sci. Res.* **4**, 365–373 (2013).
33 Kar, S., Talukdar, S., Pal, S., Nayak, S., Paranjape, P. & Kundu, S. C. Silk gland fibroin from Indian muga silkworm Antheraea assama as potential biomaterial. *Tissue Eng. Regen. Med.* **10**, 200–210 (2013).
34 Mandal, B. B. & Kundu, S. C. Osteogenic and adipogenic differentiation of rat bone marrow cells on non-mulberry and mulberry silk gland fibroin 3D scaffolds. *Biomaterials* **30**, 5019–5030 (2009).
35 Bhardwaj, N., Sow, W. S., Devi, D., Ng, K. ,W., Mandal, B. B. & Cho, N. J. Correction: Silk fibroin–keratin based 3D scaffolds as a dermal substitute for skin tissue engineering. *Integr. Biol.* **7**, 142–151 (2015).
36 Aurand, R. E., Wagner, J. L., Shandas, R. & Bjugstad, K. B. Hydrogel formulation determines cell fate of fetal and adult neural progenitor cells. *Stem Cell Res.* **12**, 11–23 (2014).
37 Bhardwaj, N. & Kundu, S. C. Silk fibroin protein and chitosan polyelectrolyte complex porous scaffolds for tissue engineering applications. *Carbohydr. Polym.* **85**, 325–335 (2011).
38 Datta, A., Ghosh, A. K. & Kundu, S. C. Differential expression of the fibroin gene in developmental stages of silkworm, *Antheraea mylitta* (Saturniidae). *Comp. Biochem. Physiol. B* **129**, 197–204 (2001).
39 Silva, N. A., Cooke, N. J., Tam, R. Y., Sousa, N., Salgado, A. J., Reis, R. L. & Shoichet, M. S. The effects of peptide modified gellan gum and olfactory ensheathing glia cells on neural stem/progenitor cell fate. *Biomaterials* **33**, 6345–6354 (2012).
40 Park, H., Larson, B. L., Kolewe, M. E., Vunjak-Novakovic, G. & Freed, L. E. Biomimetic scaffold combined with electrical stimulation and growth factor promotes tissue engineered cardiac development. *Exp. Cell Res.* **321**, 297–306 (2014).
41 Subia, B., Dey, T., Sharma, S. & Kundu, S. C. Target specific delivery of anticancer drug in silk fibroin based 3D distribution model of bone – breast cancer cells. *ACS Appl. Mater. Interfaces* **7**, 2269–2279 (2015).